Superfluorinated and NIR-luminescent gold nanoclusters†

V. Dichiarante‡ [ab], I. Tirotta‡ [abc], L. Catalano [b], G. Terraneo [ab], G. Raffaini [b], M. R. Chierotti [d], R. Gobetto [d], F. Baldelli Bombelli *[ab] and P. Metrangolo *[abce]

[a]*Fondazione Centro Europeo Nanomedicina, Politecnico di Milano, Milan, Italy*

[b]*Department of Chemistry, Materials, and Chemical Engineering "Giulio Natta", Politecnico di Milano, Milan, Italy. E-mail:* francesca.baldelli@polimi.it; pierangelo.metrangolo@polimi.it

[c]*Center for Nano Science&Technology IIT@POLIMI (CNST), Milan, Italy*

[d]*Department of Chemistry and NIS, University of Turin, Italy*

[e]*VTT-Technical Research Centre of Finland Ltd, Espoo, Finland*

A novel class of superfluorinated and NIR-luminescent gold nanoclusters were obtained starting from a branched thiol, bearing 27 equivalent ^{19}F atoms per molecule. These unprecedented clusters combine in a unique nanosystem both NIR photoluminescence and ^{19}F NMR properties, thus representing a promising multimodal platform for bioimaging applications.

Metal clusters around 2 nm show interesting and useful size-dependent properties, which greatly differ from those of larger nanoparticles, bulk metals, or single atoms.[1] Gold nanoclusters (AuNCs) passivated by thiols, $Au_n(SR)_m$, are among the most studied because of their high stability.[2a] Furthermore, AuNCs do not show plasmon UV-vis resonances, but are characterized by a strong luminescence in the near infrared (NIR) region, which makes them perfect candidates for *in vivo* optical imaging.[4a] Most of the studied AuNCs are stabilized by simple alkane- or arenethiols, though more complex, bulky ligands are also valuable for introducing important functionalities.[6a] In fact, various bulky or structurally complex thiols (*e.g.*, drug analogues, cyclodextrin derivatives, DNA oligonucleotides, polymers, dendrimers, calixarenes, and proteins, among others) have been used to produce AuNCs for various applications, such as sensing, diagnostics and drug delivery.[8–12]

In recent years, fluorinated ligands have increasingly been exploited for the development of various types of nanoparticles (NPs), which yielded new materials with enhanced chemical features, such as corrosion resistance, anti-fouling properties, catalytic activity, *etc.*[13–16] Fluorinated gold NPs (*i.e.*, F-AuNPs), in particular, have found large use as powerful bioimaging tools.[17–19]Most of the reported F-AuNPs are functionalized by long-chain linear perfluoroalkyl ligands, which resulted in the formation of particles in the 2–4 nm size range.[2a] One of the viable strategies to obtain smaller fluorinated AuNCs (F-AuNCs) requires the use of bulkier ligands based on branched fluorinated molecules.[2] In this regard, short-chain and branched fluorinated ligands represent a more sustainable replacement of their linear counterparts, which have raised substantial concerns for their environmental impact and bioaccumulation. Here we report a novel class of AuNCs stabilized by a superfluorinated bulky thiol (Fig. 1).

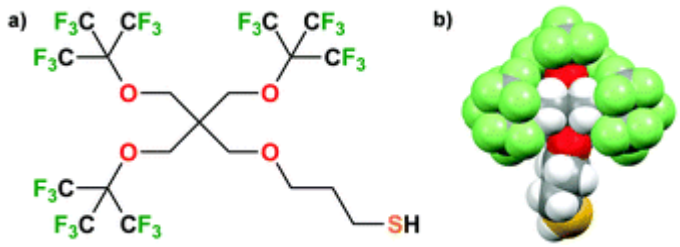

Fig. 1 Chemical drawing (a) and single crystal X-ray structure (b) of thiol **1**.

Ligand **1** (Fig. 1a) was designed on the basis of PERFECTA,[21] a pentaerythritol-based superfluorinated (SF) contrast agent for ^{19}F Magnetic Resonance Imaging (MRI), containing 36 magnetically equivalent fluorine atoms. One of the four pentaerythrityl arms has been functionalized with a thiol-terminated chain for enabling binding to an Au surface (Fig. 1a).[22] The functionalization of a single arm was verified by NMR studies (see the ESI† and later) and confirmed by single crystal X-ray diffraction analysis.

The crystal structure of thiol **1** (Fig. 1b) highlights the superfluorinated and branched nature of this ligand, which shows two distinct sections: the bulky SF head and the hydrogenated alkyl tail. Interestingly, in the solid state, the alkyl tail adopts a rather extended conformation protruding from the SF head. This arrangement leaves the thiol group outwardly oriented and available for further coupling to the Au surface. The supramolecular organization of ligand **1** molecules in the crystal is driven by several F···F interactions among CF_3 groups of adjacent molecules (F···F distances in the range of 2.8–2.9 Å) and weak H···F contacts involving the hydrogenated tail. As a consequence of these rather weak interactions, the overall crystal lattice is quite unstable and all the measured crystals experienced fast decay.

In order to foresee the role of these weak van der Waals interactions in the stabilization on a shell of SF thiols around an AuNC, we performed Molecular Mechanics (MM) and Molecular Dynamics (MD) simulations. For investigating the possible conformations displayed by the fluorinated chains and evaluate the steric hindrance at a non-flat interface, we modelled at first an ideal nanocluster-sized Au sphere of about 1 nm diameter.[23] Various fluorinated chains, from four to eight, were covalently bound to the surface (details are reported in the ESI†). Using a simulation protocol adopted in previous works and based on MM-MD methods,[23,24] we obtained a final optimized geometry of the Au nanosphere at room temperature. An interesting energetic stabilization was found increasing the number of fluorinated chains bound to the surface, due to F···F interactions among neighbouring chains (see Fig. 2a). In particular, the energy gain normalized by the number of fluorinated chains kept increasing up to five and six bound molecules, while it became somewhat smaller for seven and eight molecules, due to an increase in steric repulsions. The radial distribution function reported in Fig. 2b shows the distribution of the fluorine atoms as a function of the distance *r* from the center of mass (c.o.m.) of the ideal gold nanosphere. Around this Au core the fluorine atoms are distributed in the distance range between 6 and 18 Å. The observed separations in the fluorine atom below 3.0 Å, equivalent to the sum of the van der Waals radii of two F atoms,[25] are indicative of stabilizing interactions between the fluorinated chains.

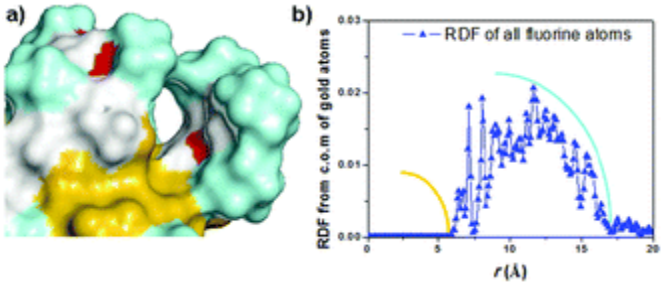

Fig. 2 Theoretical modelling of molecules of **1** covalently bound to an ideal Au nanosphere (a), and Radial Distribution Function (RDF) of all fluorine atoms of the ligands with respect to the center of mass, c.o.m., of the model nanosphere (b).

Ligand **1** was successfully used to produce SF-AuNCs. In particular, we followed a procedure described by Dass *et al.* for producing 1*H*,1*H*,2*H*,2*H*-perfluorodecanethiol (PFDT)-stabilized AuNCs by using a slightly modified Brust reaction.[20] The protocol was optimized on PFDT by obtaining **PFDT-AuNCs** with a mean diameter of 2.3 ± 0.7 nm, which we used as the reference for comparison with the new branched system (see the ESI† for detailed experimental data). The same reaction performed with ligand**1** (1 : 3 Au : thiol ratio) resulted in smaller clusters (**SF-AuNCs1**) with a mean diameter of 1.4 ± 0.6 nm as evidenced by TEM analysis (Fig. 3a and b). This smaller size is a likely consequence of the larger molecular volume occupied by the branched thiol **1**(515 Å^3) compared to PFDT (326 Å^3).§ As expected, increasing the amount of fluorinated thiol **1** in the synthesis up to 6 equivalents seemed to lead to a further decrease of the core mean diameter to 1.1 ± 0.6 nm (**SF-AuNCs2**; see the ESI† for detailed characterization).

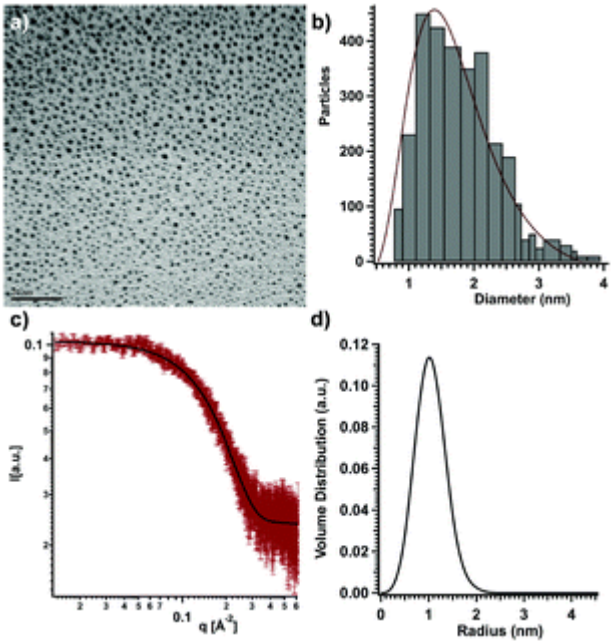

Fig. 3 TEM image (a), with relative statistical analysis (b) of a dispersion in 1,1,1,3,3-pentafluorobutane of **SF-AuNCs1**. SAXS spectrum (c) of **SF-AuNCs1** in 1,1,1,3,3-pentafluorobutane, where the black curve is the best fitting curve using a form factor of polydisperse core–shell spheres, and volume distribution of radius size (d) from SAXS obtained by GIFT.

A size distribution analysis on **SF-AuNCs1** dispersed in 1,1,1,3,3-pentafluorobutane was carried out using Small Angle X-ray Scattering (SAXS; Fig. 3c and d). First, the SAXS curve was analysed using a form factor of polydisperse spherical particles with a core–shell structure (solid curve in Fig. 3c) that resulted in an average Au core radius of 0.9 nm, a fluorinated shell thickness of 0.3 nm and a Schultz polydispersity of 0.2.[21] This was also confirmed using the GIFT program[22] to invert the SAXS spectrum and obtain the pair-distance distribution function (PDDF) assuming a homogeneous spherical shape. The obtained size distribution reported in Fig. 3d shows a well-dispersed population of single AuNCs of an average size of about 2 nm, which is in good agreement with the size obtained by TEM analysis.

Differently from **PFDT-AuNCs** (see the ESI†), UV-vis absorption spectra of both **SF-AuNCs1** (Fig. 4a) and **SF-AuNCs2** (Fig. S9, ESI†) dispersed in 1,1,1,3,3-pentafluorobutane showed a step-like fine structure. This molecule-like optical behaviour is typical of NCs with core sizes below 2 nm. In particular, prominent absorption features were observed at 680, 442, 400, and 320 nm, which are well-known features of the Au_{25} cluster core.[3,20,23] MALDI mass analysis was

also performed to determine the number of gold atoms per ligand molecule in **SF-AuNCs1** (see Fig. S12, ESI†). The most prominent peak at the highest mass was found at m/z = 16 166; however, many other peaks of lower intensities were also present at lower m/z values. This is not unexpected, taking into account both the polydispersity of the sample and the fact that, typically, extensive core and ligand fragmentations are observed in MALDI mass analysis of NCs.[31] Interestingly, interpreting the peak at m/z = 16 166 as related to an Au_{25} core would indicate a ligand shell of 13 ligands. This stoichiometry is rather unusual for Au_{25} NCs, which most commonly feature 18 thiols, and may be related to the bulkiness of our SF thiol **1**, as modelled by the MM–MD simulations. However, further investigations are needed to definitely assess the number of gold atoms per ligand molecule in **SF-AuNCs1**, and confirm the rather peculiar $Au_{25}(SR)_{13}$ stoichiometry.

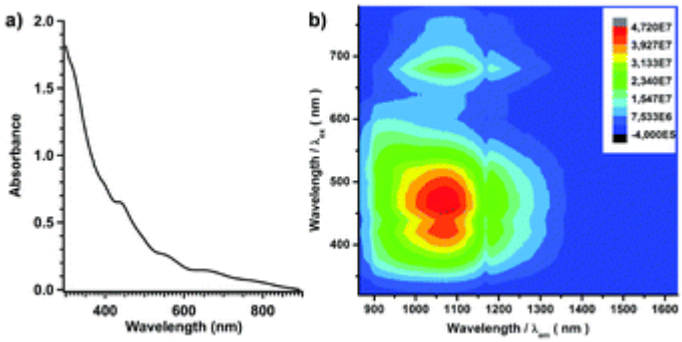

Fig. 4 UV-vis spectrum of **SF-AuNCs1** in 1,1,1,3,3-pentafluorobutane (a), and their full luminescence 3D spectrum (b), showing emission wavelength (x axis), excitation wavelength (y axis), and intensity (z axis).

Both SF-AuNCs displayed an intense photoluminescence in the NIR region (Fig. 4b and Fig. S11, ESI†). In particular, excitation of the SF-AuNC dispersions between 380 and 520 nm gave a strong emission centred at 1050 nm. For **SF-AuNCs1**, the excitation wavelength could be moved up to 700 nm, still maintaining a detectable luminescence in the 1000–1100 nm region (Fig. 4b). The quantum yield of **SF-AuNCs1** was estimated to be 12% for the lower excitation wavelength. The possibility of exciting in the NIR region (650–1350 nm), also known as the therapeutic window, is of paramount importance in optical bioimaging applications. At these wavelengths, in fact, it is possible to maximise light's tissue penetration depth. Moreover, emission in the NIR spectral region avoids interference from most biological chromophores, allowing selective detection of the imaging probe's luminescence.[32]

The Nuclear Magnetic Resonance properties of the obtained SF-AuNCs were also studied. As expected, the ^{19}F NMR spectrum of thiol **1** (recorded in 1,1,1,3,3-pentafluorobutane, Fig. 5a) shows a sharp, very intense, single resonance peak at −71.15 ppm. Its relaxivity properties are also promising, with a relatively short T_1 and a very long T_2 (Table S3, ESI†), indicating high suitability for ^{19}F MRI. ^{19}F NMR spectra of both **SF-AuNCs1** and **SF-AuNCs2** dispersions in 1,1,1,3,3-pentafluorobutane displayed an intense peak at the same chemical shift of thiol **1**, plus two other smaller peaks at −70.96 and −71.04 ppm (Fig. 5b). The major peak at −71.14 ppm is very sharp and intense, thus allowing for artefact-free MR images, and the relaxivity properties are well in line with the most successful fluorinated contrast agents reported in the literature, so far (Table S3, ESI†). On the other hand, the smaller peaks may due to the size distribution of the sample, where various SF-AuNCs of diameters between 0.8 and 2 nm are present in solution (mean diameter 1.4 ± 0.6 nm). The magnetic performance of our

novel SF-AuNCs makes them suitable for ^{19}F-MRI application, which along with the very strong NIR emission allows us to envision their potential application in bioimaging as a dual modality platform.

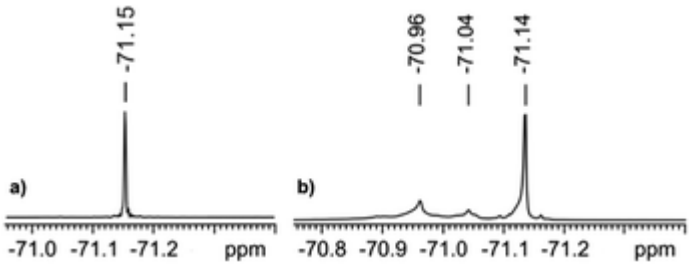

Fig. 5 ^{19}F (564.73 MHz) NMR spectra of thiol **1** (a) and **SF-AuNCs1** (b) in 1,1,1,3,3-pentafluorobutane (C_6D_6 capillary used for locking).

The biological application of such a system requires dispersion of SF-AuNCs in water, for example by using biocompatible surfactants. Thus, 1,2-dioleoyl-*sn*-*glycero*-3-phosphocholine (DOPC) liposomal dispersions of SF-AuNCs were studied. Briefly, pentafluorobutane-dispersed NCs were added to a solution of DOPC in chloroform and the mixture was dried under vacuum. The dried film was re-dispersed in aqueous solution and subjected to size reduction procedures. Successful encapsulation was confirmed *via* Inductively Coupled Plasma Mass Spectrometry (ICP-MS) analysis, which showed, on an average, an Au concentration of 26 mg L^{-1}, corresponding to 7.74×10^{14} NCs ml^{-1}. Multiangle Dynamic Light Scattering (DLS) analysis of the final liposomal dispersion showed an averaged hydrodynamic radius of 69 nm, similar to the unloaded liposomal system (see the ESI† for detailed characterization). **SF-AuNCs1**-loaded liposomes displayed a photoluminescence behaviour very similar to that observed for the same clusters in pentafluorobutane-based solutions (Fig. 6a) with the emission peak at λ_{exc} = 700 nm still clearly visible, although decreased in intensity. The ^{19}F-NMR spectrum of the liposomal dispersion displayed two peaks probably indicating different domains of the **SF-AuNCs1** in the liposomal dispersions (Fig. 6b) with the major one at 71.90 ppm. Further optimization of these formulations is needed for their use in biological applications, but although preliminary, these results show the possibility of easily preparing biocompatible aqueous formulations of the developed **SF-AuNCs**.

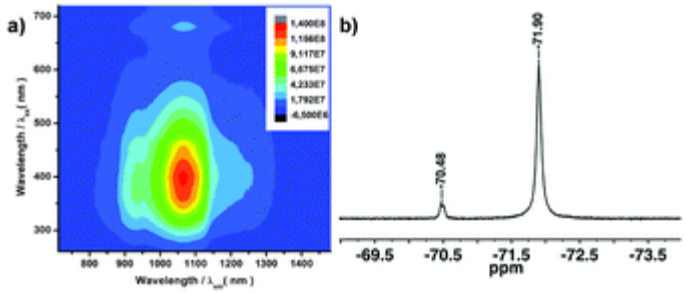

Fig. 6 Full luminescence 3D spectrum of a DOPC-based liposomal dispersion of **SF-AuNCs1** in MilliQ water (a), showing the emission wavelength (*x* axis), the excitation wavelength (*y* axis) and the intensity (*z* axis). (b) ^{19}F NMR spectrum of the same sample, with D_2O added for locking.

In conclusion, we have reported a novel class of superfluorinated and highly branched AuNCs. This novel class of nanosystems showed excellent NIR photoluminescence properties, with an emission maximum centred at 1050 nm when excited between 460 nm and 680 nm, as well as a very sharp and intense ^{19}F

NMR peak at −71.14 ppm. The same characteristics were maintained when the developed NCs were successfully dispersed in water by using a commercially available, biocompatible liposomal formulation. As a consequence, we believe that the reported SF-AuNCs may represent a novel and efficient platform for multimodal bioimaging applications. Optimization of the liposomal dispersion of the obtained SF-AuNCs is currently under way in our laboratories and will be reported elsewhere.

Regione Lombardia (Fondo per lo Sviluppo e la Coesione, FAS 2007–2013) is acknowledged for financial support. R. G. and M. R. C. acknowledge the Jeol Company for the fruitful collaboration. The authors are also grateful to Dr S. Perissinotto (CNST-IIT, Milan) for technical support with photoluminescence experiments, Dr R. Milani (VTT, Espoo) for MALDI analysis, and the staff at Anton Paar (Graz) for SAXS measurements.

Notes and references

1. J. P. Wilcoxon and B. L. Abrams, *Chem. Soc. Rev.*, 2006, **35**, 1162–1194
2. D. M. Chevrier, R. Yang, A. Chatt and P. Zhang, *Nanotechnol. Rev.*, 2015, **4**, 193–206
3. R. Jin, *Nanoscale*, 2015, **7**, 1549–1565
4. L. Zhang and E. Wang, *Nano Today*, 2014, **9**, 132–157
5. L.-Y. Chen, C.-W. Wang, Z. Yuan and H.-T. Chang, *Anal. Chem.*, 2015, **87**, 216–229.
6. Y. Pei and X. C. Zeng, *Nanoscale*, 2012, **4**, 4054–4072.
7. P. J. Krommenhoek, J. Wang, N. Hentz, A. C. Johnston-Peck, K. A. Kozek, G. Kalyuzhny and J. B. Tracy, *ACS Nano*, 2012, **6**, 4903–4911.
8. S. Palmal and N. R. Jana, *Wiley Interdiscip. Rev.: Nanomed. Nanobiotechnol.*, 2014, **6**, 102–110.
9. J. Li, J.-J. Zhu and K. Xu, *Trends Anal. Chem.*, 2014, **58**, 90–98.
10. Y. Kong, J. Chen, F. Gao, R. Brydson, B. Johnson, G. Heath, Y. Zhang, L. Wua and D. Zhou, *Nanoscale*, 2013, **5**, 1009–1017.
11. J. Xie, Y. Zheng and J. Y. Ying, *J. Am. Chem. Soc.*, 2009, **131**, 888–889.
12. K. Chaudhari, P. Lourdu Xavier and T. Pradeep, *ACS Nano*, 2011, **5**, 8816–8827.
13. D. J. Weinberg, C. He and E. A. Weiss, *J. Am. Chem. Soc.*, 2016, **138**, 2319–2326.
14. H. Zhou, H. Wang, H. Niu, A. Gestos, X. Wang and T. Lin, *Adv. Mater.*, 2012, **24**, 2409–2412.
15. H. Wang, J. Fang, T. Cheng, J. Ding, L. Qu, L. Dai, X. Wang and T. Lin, *Chem. Commun.*, 2008, 877–879.
16. J.-D. Brassard, D. K. Sarkar and J. Perron, *ACS Appl. Mater. Interfaces*, 2011, **3**, 3583–3588.
17. M. E. Kurczy, Z.-J. Zhu, J. Ivanisevic, A. M. Schuyler, K. Lalwani, A. F. Santidrian, J. M. David, A. Giddabasappa, A. J. Roberts, H. J. Olivos, P. J. O'Brien, L. Franco, M. W. Fields, L. P. Paris, M. Friedlander, C. H. Johnson, A. A. Epstein, H. E. Gendelman, M. R. Wood, B. H. Felding, G. J. Patti, M. E. Spilker and G. Siuzdak, *Nat. Commun.*, 2015, **6**(5998), 1–8.
18. M. Boccalon, P. Franchi, M. Lucarini, J. J. Delgado, F. Sousa, F. Stellacci, I. Zucca, A. Scotti, R. Spreafico, P. Pengo and L. Pasquato, *Chem. Commun.*, 2013, **49**, 8794–8796.
19. M. Şologan, D. Marson, S. Polizzi, P. Pengo, S. Boccardo, S. Pricl, P. Posocco and L. Pasquato, *ACS Nano*, 2016, **10**, 9316–9325.
20. P. Pengo and L. Pasquato, *J. Fluorine Chem.*, 2015, **177**, 2–10.
21. I. Tirotta, A. Mastropietro, C. Cordiglieri, L. Gazzera, F. Baggi, G. Baselli, M. G. Bruzzone, I. Zucca, G. Cavallo, G. Terraneo, F. Baldelli Bombelli, P. Metrangolo and G. Resnati, *J. Am. Chem. Soc.*, 2014, **136**, 8524–8527.
22. X. Yue, M. B. Taraban, L. L. Hyland and Y. B. Yu, *J. Org. Chem.*, 2012, **77**, 8879–8887.
23. G. Raffaini and F. Ganazzoli, *Langmuir*, 2003, **19**, 3403–3412.
24. G. Raffaini, L. Melone and C. Punta, *Chem. Commun.*, 2013, **49**, 7567–7570.
25. S. Alvarez, *Dalton Trans.*, 2013, **42**, 8617–8636.
26. A. Dass, R. Guo, J. B. Tracy, R. Balasubramanian, A. D. Douglas and R. W. Murray, *Langmuir*, 2008, **24**, 310–315.
27. J. Hayter, in *Physics of Amphiphiles: Micelles, Vesicles and Microemulsions*, ed. V. Degiorgio and M. Corti, North Holland, Amsterdam, 1983, p. 69.
28. O. Glatter, *J. Appl. Crystallogr.*, 1980, **13**, 577–584.
29. H. Qian, M. Zhu, Z. Wu and R. Jin, *Acc. Chem. Res.*, 2012, **45**, 1470–1479.
30. J. Hassinen, P. Pulkkinen, E. Kalenius, T. Pradeep, H. Tenhu, H. Häkkinen and R. H. A. Ras, *J. Phys. Chem. Lett.*, 2014, **5**, 585–589.
31. A. J. Arnold and J. P. Reilly, *J. Am. Chem. Soc.*, 1998, **120**, 1528–1532.
32. J. V. Frangioni, *Curr. Opin. Chem. Biol.*, 2003, **7**, 626–634